CrystEngComm

Cite this: *CrystEngComm*, 2011, **13**, 6801

www.rsc.org/crystengcomm

PAPER

Solvent-mediated crystal-to-crystal transformation within the $CoBr_2$(1,4-dioxane)$_m$(H_2O)$_n$ family (m = 2, 3; n = 0, 2, 4) from 2D to 1D, and 0D†

Zhiming Duan,[ab] Yan Zhang,[c] Bin Zhang*[a] and Daoben Zhu*[a]

Received 2nd June 2011, Accepted 3rd August 2011
DOI: 10.1039/c1ce05668a

A family of coordination compounds: $CoBr_2$(1,4-dioxane)$_2$ (**1**), $CoBr_2$(1,4-dioxane)$_2$(H_2O)$_2$ (**2**), $CoBr_2$(1,4-dioxane)$_3$(H_2O)$_4$ (**3**) and $CoBr_2$(1,4-dioxane)$_2$(H_2O)$_4$ (**4** (*C* 2/c) and **5** (*I* 4_1/a)) with different dimensions have been crystallized from a solution of CH_3OH/1,4-dioxane. The solvent-mediated transformation was observed from the blue kinetically favored 2D compound **1** to the red metastable 1D compound **2**, 0D compound **3**, and finally to the thermodynamically stable 0D compounds **4** and **5**. The hydrogen bonds played a key role in the formation of the different networks of **2–5** with the increasing of the coordinated water molecules. The magnetic measurements showed that **1** was a canted antiferromagnet, and **3–5** acted as antiferromagnets.

Introduction

Metal organic frameworks (MOFs) have received much attention in the past decades due to their intriguing structures and potential applications.[1] Recently there has been growing interest in the exploration of new MOFs showing promising properties for gas adsorption, catalysis, chemical sensing, second-order nonlinear optical (NLO), molecular magnetic and ferroelectric materials.[2] In the field of crystal engineering, precise prediction of the structure of supramolecular assemblies for applications in the above areas is still very difficult, because many weak non-covalent intermolecular forces govern the packing of molecular building blocks in the solid state.[3] Among those governing factors, hydrogen bonding may play an important role in the formation of functional materials.[4] The strength and arrangement of the hydrogen bonds could not only have an influence on the self-assembly process, but also affect the orientations of the building blocks. Therefore, hydrogen bonds are extensively adopted in many interesting systems including MOFs.[5]

The tuning effect of the hydrogen bonding is often realized by solution chemistry, but the understanding of the framework formation in the solution state is limited.[6] There is no suitable model for explaining the subtle kinetic and thermodynamic driving forces during the crystal nucleation and growth process, and there will be a good chance to learn some rules from investigations on the dynamic structural transformation of the metastable crystals. The transformation from a metastable form to a stable one can be described by a solid state (crystal to crystal) or a solvent-mediated mechanism.[7,8] There has been increasing attention in the research of the latter mechanism, mainly because it may promote a better understanding of the crystallization courses and be used to prepare a new class of materials with attractive properties. S. Rizzato *et al.* have undertaken a systematic study of the MCl_2/1,3-bis(4-pyridyl)propane (bpp) system, and they have shown that the correct use of crystallization techniques allows tuning of the metal to ligand ratio and absolute concentrations and, hence, control of the crystallization of the MCl_2/bpp couple based MOFs, including their solvent-mediated phase transitions.[9]

Our recent studies on the MCl_2/1,4-dioxane/H_2O system have shown it to be a good candidate for the dynamic crystal. The crystal-to-crystal transformation involves changes in the dimensionality, color, and physical properties. In this system, Cl^-, 1,4-dioxane and H_2O can serve as terminal or bridging ligands, 1,4-dioxane and H_2O can even serve as a guest molecules. The diversity results in flexible structures with interesting hydrogen bonding networks.[10] A subtle tuning of the MCl_2/1,4-dioxane/H_2O ratio could lead to a vast change in the arrangement of the hydrogen bonding, and have an impact on the formation of the final structures. To improve understanding of the self-assembly processes of coordination networks, we pay our attention to the MBr_2/1,4-dioxane/H_2O system. We investigate the solvent-mediated crystal-to-crystal transformation on $CoBr_2$/1,4-dioxane/H_2O system, a family of $CoBr_2$(1,4-dioxane)$_m$(H_2O)$_n$ (m = 2 or 3, n = 0, 2 or 4), where the interplaying of the experimental conditions, their structures, magnetic properties

[a]*Organic Solid Laboratory, BNLMS, CMS & Institute of Chemistry, Chinese Academy of Sciences, Beijing, 100190, P. R. China. E-mail: zhangbin@iccas.ac.cn; zhudb@iccas.ac.cn; Fax: +86-10-62559373 (B. Zhang); +62544083 (D. Zhu); Tel: +86-10-62558982 (B. Zhang); +62544083 (D. Zhu)*
[b]*Graduate School, Chinese Academy of Sciences, Beijing, 100049, P. R. China*
[c]*Institute of Condensed Matter and Material Physics, Department of Physics, Peking University, Beijing, 100871, P. R. China*
† Electronic supplementary information (ESI) available: structural relationships, IR spectra, TGA plots and XPRD plots. CCDC reference numbers 802394–802398. For ESI and crystallographic data in CIF or other electronic format see DOI: 10.1039/c1ce05668a

and solvent-mediated crystal-to-crystal transformations are reported here.

Experimental details

All reagents were obtained from commercial sources and were used as received without further purification.

$CoBr_2 \cdot xH_2O$ (100 mg) was dissolved in a mixture of CH_3OH (1.0 mL) and 1,4-dioxane (4.0 mL). Blue plate-shaped crystals of **1** were obtained by slow solvent evaporation in a desiccator or exposure to ambient air at relative humidity (RH) lower than 40% for about two weeks. The crystal is unstable in air with the color changing from blue to red when exposed to air. Elemental analysis calcd (%) for $C_8H_{16}O_4CoBr_2$ (394.95): C 24.33, H 4.08; found: C 24.03, H 4.08. An IR experiment was carried out promptly on the fresh crystal, and a small area of crystal remained blue during the experiment. IR: 3200–3400brs, 3005m, 935m, 2914m, 2877m, 2857m, 2755w, 2696w, 2360w, 2336w, 2290w, 1607s, 1456m, 1437m, 1374w, 1295m, 1252s, 1103s, 1068s, 1043m, 896m, 862s (Fig. S1†).

When **1** was kept in the mother liquor at RH higher than 50% for about one week, the blue crystal transferred slowly into red block-shaped crystals of **2**. It not possible to obtain a pure phase of **2** as it always coexisted with **1** and **4** and was very unstable in air, so characterization except IR and X-ray single crystal diffraction experiments failed. The IR experiment was carried out as soon as possible and a small area of crystal remained unchanged during the experiment. IR: 3000–3700(brs), 3002s, 2987s, 2960s, 2924s, 2900s, 2894s, 2861s, 2761m, 2698m, 2761m, 2698m, 2389m, 2360m, 2332m, 2295m, 2198m, 2149m, 2129m, 2090m, 2075m, 1961w, 1948w, 1940w, 1899w, 1888w, 1867w, 1631s, 1555m, 1540m, 1521m, 1504m, 1453s, 1438s, 1370s, 1296s, 1258s, 1105s, 1078s, 1044s, 908m, 889s, 866s (Fig. S1†).

When **1** was kept in the mother liquor at RH higher than 60% for about one week, red needle-shaped crystals of **3** were obtained. Elemental analysis calcd (%) for $C_{12}H_{32}O_{10}CoBr_2$ (555.2): C 25.96, H 5.81; found: C 26.09, H 5.80. The IR experiment failed due to the instability of a single crystal when exposed to air.

When **2** or **3** were kept in the mother liquor at RH higher than 50% for a further week, red plate-shaped crystals of **4** were obtained. After standing in the mother liquor at RH higher than 50% for a long time, **2** or **3** can be completely transformed into red prismatic crystals of **5**.[11] Elemental analysis calcd (%) for **4** and **5**, $C_8H_{24}O_8CoBr_2$ (467.01): C 20.57, H 5.18; found: C 20.48, H 5.13 (**4**) and C 20.20, H 5.11 (**5**). IR experiments on fresh single crystals of **4** and **5** (cm^{-1}): 3100–3500(brs), 2985s, 2922s, 2905s, 2892s, 2859s, 2762m, 2698m, 2587w, 2360m, 2331m, 2285m, 2202m, 2141m, 1963m, 1942m, 1900w, 1719m, 1631s, 1453s, 1370s, 1298m, 1257s, 1109s, 1080, 1045s, 888s, 868s (Fig. S1†).

Thermogravimetric analysis was carried out on a Shimadzu DTG-60 Analyzer with 10 °C min^{-1} from room-temperature to 600 °C on **1**, **3**, and **5** successfully (Fig. S2†). The desolvation procedures of them could be estimated from mass loss and the stoichiometries were proposed tentatively: **1** was desolvated into $CoBr_2$ at 116 °C (56% remained). **3** was desolvated into $CoBr_2(1,4\text{-dioxane})_2(H_2O)_4$ at 97 °C with 1/3 of 1,4-dioxane lost (85% remained), 2/3 of 1,4-dioxane molecule desolvated above 178 °C (53% remained), $CoBr_2(H_2O)_4$ was dehydrated into $CoBr_2$ (39% remained) at 212 °C. **5** decomposed into $CoBr_2$(1,4-dioxane)(H_2O) from 30 to 97 °C with half of 1,4-dioxane and 3/4 of H_2O lost (70% remained). From 97 to 135 °C, H_2O dehydrated from $CoBr_2$(1,4-dioxane)(H_2O) (65% remained), and 1,4-dioxane desolvated around 200 °C (47% remained).

Powder X-ray diffraction patterns were obtained on a Rigaku RINT2000 diffractometer at room temperature with Cu-Kα radiation in a flat-plate geometry with crystal covered with paraffin liquid. **1**, **2** and **3** failed in PXRD due to instability. The experimental PXRD patterns of **4**, **5** matched well with the calculated ones based on the single-crystal structures (Fig. S3†), confirming the phase purity of **4** and **5**.

Single Crystal X-ray diffraction data was collected at 293 K on a Nonius KappaCCD or 173 K on a Rigaku diffractometer with graphite monochromated Mo-Kα radiation (λ = 0.71073 Å).[12] The structures were solved by direct method and refined by full-matrix least-squares on F^2 using the SHELX program, with anisotropic thermal parameters for all non-hydrogen atoms.[13] Hydrogen atoms of H_2O were found by difference Fourier and refined isotropically. Hydrogen atoms of 1,4-dioxane were located by calculation and refined isotropically. The crystallographic data of **1–5** are listed in Table 1. The selected bond lengths and hydrogen bonds are listed in Table 2. CCDC 802394–802398 contain the supplementary crystallographic data for this paper.†

Magnetization measurements were performed against tightly packed polycrystalline samples in capsules on a Quantum Design MPMS 7XL SQUID system. Susceptibility data were corrected for diamagnetism of the samples by Pascal constants (-137.6×10^{-6} cm^3 mol^{-1} for **1**, -302.4×10^{-6} cm^3 mol^{-1} for **3**, and -246.0×10^{-6} cm^3 mol^{-1} for **4** and **5**) and background by experimental measurement on the sample holder.[14] The magnetic characterization of **2** failed due to the problem of purity.

Results and discussion

1 crystallizes in tetragonal with space group $I\,4_1/a$. The asymmetric unit consists of half of Co(II), two of half monodentate Br^- and one 1,4-dioxane molecule. Co(II) locates on the 4_1 screw axis and adopts a nearly regular octahedral geometry. As shown in Fig. 1a, four 1,4-dioxane molecules are bound to Co(II) in the equatorial plane (Co–O bond lengths of 2.151(4) and 2.162(4) Å) and two Br^- are bound to Co(II) from axial sites (Co–Br bond lengths of 2.543(1) and 2.561(1) Å) as shown in Table 2. In **1**, 1,4-dioxane adopts a chair configuration and links two Co(II) with an end-to-end bridging mode, resulting in a two-dimensional (2D) layer with a (4,4) topology parallel to the *ab* plane (shown in Fig. 1b). The dimensions of the square *ca.* 7.1 × 7.1 $Å^2$ (the Co–Co separations) are comparable with the size of the square grids observed in other related complexes.[15] The perpendicular separation between the mean plane of the neighboring layers is 5.83 Å. Layers align along the *c* axis in a slipped arrangement give an AB packing mode (Fig. 1c). The AB stacking of the square-grid layers prevents substantial void space in the structure. This packing arrangement may be explained by the existence of C···Br short contacts (*ca.* 3.62 to 3.72 Å) between the neighboring layers.

2 belongs to triclinic with space group $P\bar{1}$. Co(II) adopts a compressed octahedral geometry with two monodentate Br^-

Table 1 Crystallographic Data of **1–5**

Compound	**1**	**2**	**3**	**4**	**5**
Formula	$CoBr_2$(1,4-dioxane)$_2$	$CoBr_2$(1,4-dioxane)$_2$(H_2O)$_2$	$CoBr_2$(1,4-dioxane)$_3$(H_2O)$_4$	$CoBr_2$(1,4-dioxane)$_2$(H_2O)$_4$	$CoBr_2$(1,4-dioxane)$_2$(H_2O)$_4$
Color	Blue	Purple	Red	Red	Red
Fw	394.96	430.98	555.12	467.02	467.02
F(000)	1544	213	932	3728	932
T/K	200	173	173	293	293
Crystal system	Tetragonal	Triclinic	Triclinic	Monoclinic	Tetragonal
Space group	$I\,4_1/a$	$P\bar{1}$	$P\bar{1}$	$C\,2/c$	$I\,4_1/a$
Cell parameters	$a = 10.0681(3)$ Å $b = 10.0681(3)$ Å $c = 23.396(1)$ Å $\alpha = 90°$ $\beta = 90°$ $\gamma = 90°$ $V = 2371.6(1)$ Å^3	$a = 5.821(2)$ Å $b = 6.978(2)$ Å $c = 10.275(3)$ Å $\alpha = 99.636(3)°$ $\beta = 101.641(3)°$ $\gamma = 112.746(2)°$ $V = 362.8(2)$ Å^3	$a = 6.460(2)$ Å $b = 9.033(2)$ Å $c = 9.738(3)$ Å $\alpha = 105.540(4)°$ $\beta = 98.341(3)°$ $\gamma = 92.690(3)°$ $V = 539.4(2)$ Å^3	$a = 23.4355(4)$ Å $b = 25.8418(6)$ Å $c = 11.7298(2)$ Å $\alpha = 90°$ $\beta = 113.109(1)°$ $\gamma = 90°$ $V = 6533.7(2)$ Å^3	$a = 9.1728(3)$ Å $b = 9.1728(3)$ Å $c = 19.5503(7)$ Å $\alpha = 90°$ $\beta = 90°$ $\gamma = 90°$ $V = 1645.0(1)$ Å^3
Z	8	1	1	16	4
D_c/g cm^{-3}	2.212	1.973	1.709	1.899	1.886
μ(Mo-Kα)/mm^{-1}	8.178	6.700	4.541	5.969	5.928
Crystal size/mm	0.05 × 0.22 × 0.32	0.13 × 0.25 × 0.27	0.16 × 0.23 × 0.32	0.13 × 0.22 × 0.28	0.28 × 0.30 × 0.40
T_{min} and T_{max}	0.259, 0.718	0.2055, 0.3237	0.0858, 0.2806	0.226,0.469	0.105,0.226
θ_{min}, θ_{max} (°)	0.993, 27.47	0.987, 30.99	0.992, 30.49	0.995, 25.09	0.998, 27.50
no. total reflns.	24605	5941	8706	42739	10060
no. uniq. reflns. (R_{int})	1354(0.0521)	2283(0.0351)	3260(0.0398)	5777(0.1059)	940(0.0910)
no. obs. [$I \geq 2\sigma(I_0)$]	723	2206	3019	2632	662
no. params.	71	86	180	392	53
R_1, wR_2 [$I \geq 2\sigma(I_0)$]	0.0410, 0.1179	0.0285, 0.0602	0.0355, 0.0683	0.0378,0.0830	0.0433, 0.1132
R_1, wR_2 (all data)	0.0868, 0.1328	0.0298, 0.0609	0.0398,0.0705	0.1012, 0.1052	0.0621, 0.1239
GOF	1.029	1.134	1.098	0.913	1.046
[a]$\Delta\rho$, e/Å^3	1.694/−0.779	0.871/−0.572	0.403/−0.463	0.500/−1.077	0.683/−0.638
[b]Max. and mean Δ/σ	0.000/0.000	0.000, 0.000	0.001, 0.000	0.001,0.000	0.000,0.000
CCDC	802394	802395	802398	802396	802397

anions (Co–Br 2.5783(5) Å) and two 1,4-dioxane (Co–O 2.156(2) Å) in the basal plane, and two H_2O at the axial sites (Co–O 2.059 (2) Å) as shown in Fig. 2a. There are two types of chair-conformed 1,4-dioxane molecules in **2**. One acts as a guest molecule, which is tilted about 37.5° to the *ab* plane. The other is an end-to-end bridging ligand, which is approximately perpendicular to the *ab* plane (the dihedral angle between the mean plane of 1,4-dioxane and the *ab* plane is about 81.5°), it links the Co(II) cations to form an infinite 1-D chain along one of the diagonals of the *ab* plane with a Co···Co separation of *ca.* 7.15 Å (shown in Fig. 2b). Moreover, monodentate Br^- interacts with the coordinated H_2O molecules of neighboring 1-D chains *via* hydrogen

Table 2 Selected bond lengths and hydrogen bonds in **1–5**

Compound	**1**	**2**	**3**	**4**	**5**
Co–O(1,4-dioxane), Å	2.162(4), 2.151(4)	2.156(2)			
Co–O(H_2O), Å		2.059(2)	2.039(2), 2.087(2)	2.058(5),2.061(4) 2.068(5),2.073(5) 2.066(4),2.071(5)	2.076(5)
Co–Br, Å	2.543(1), 2.561(2)	2.5783(5)	2.6254(5)	2.6204(9),2.6243(6),2.6213(9),2.6238(6)	2.6184(6)
C–H···Br, °/Å	3.728(7)/129.7	3.741(2)/138.5	3.232(2)/167(3)		
O–H···O, °/Å		2.757(3)/174(3)	2.758(2)/175(3) 2.771(3)/160(3) 2.762(2)/167(3)	2.745(6)/154(6) 2.774(6)/146(6) 2.790(6)/148(6) 2.740/158(6) 2.728(6)/167(7) 2.727(6)/1145(6)	3.328(4)/124(12) 3.373(4)/148(5)
O–H···Br, °/Å		3.262(2)/166(3)	3.232(2)/167(3)	3.375(4)/153(5) 3.363(4)/159(5) 3.365(4)/162(6) 3.373(4)/158(5) 3.372(4)/145(3) 3.350(4)/150(6) 3.359(4)/146(6) 3.343(4)/97(4) 3.350(4)/150(6)	3.376/150 3.324/127 3.373/112

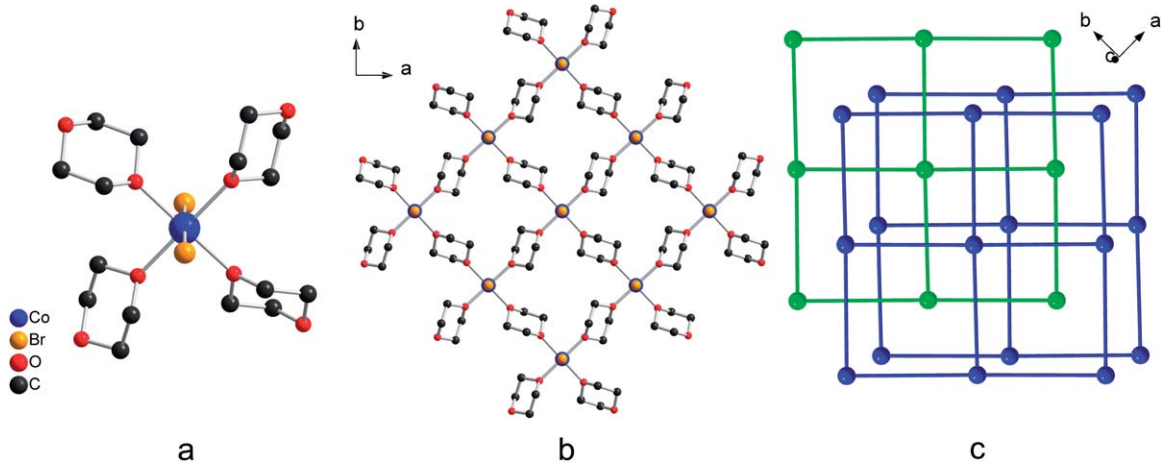

Fig. 1 a) The coordination geometry of a Co(II) cation in **1**; b) the Co(II)–Diox (4,4) layer in **1**; c) the AB stacking of the square-grid layers.

bonds (Table 2), affording a 2-D hydrogen-bonding layer (Fig. 2b). The guest 1,4-dioxane molecule intercalates into the neighboring layers (the perpendicular separation between the 2-D hydrogen-bonding layers is *ca.* 9.69 Å) *via* hydrogen bonds to form a 3-D hydrogen-bonding network (Fig. 2c). The crystal structure of **2** is different from $CuCl_2(1,4\text{-dioxane})_2(H_2O)_2$. $CuCl_2(1,4\text{-dioxane})_2(H_2O)_2$ is composed of mononuclear compounds. Cu^{2+} is octahedrally coordinated by two Cl^-, two H_2O and two O atoms (one from each of 1,4-dioxane molecules in the chair conformation) *trans* to each other. There are hydrogen bonds between mononuclear compounds.[10a,16]

3 crystallizes in triclinic with a space group of $P\bar{1}$. The Co(II) ion has a regular octahedral geometry with two monodentate Br^- (Co–Br 2.6254(5) Å) and two H_2O in the basal plane (Co–O 2.039(2) Å), two H_2O from the axial sites (Co–O 2.087(2) Å) (Fig. 3a). The neighboring mononuclear $CoBr_2(H_2O)_4$ compounds interact with each other *via* hydrogen bonds between the equatorial $Br^-$and H_2O (Table 2), affording a linear hydrogen-bonding chain along the *a* axis and the Co···Co distance is 6.46 Å (Fig. 3b). There are three types of orientations for the chair-conformed guest 1,4-dioxane molecules. In the first and second cases, the projection of the line joining two oxygen atoms in 1,4-dioxane is nearly parallel to the *b* axis. The dihedral angles between the mean planes of 1,4-dioxane and the *ab* plane are about 41.2° and 66.3°, separately. For the third one, the projection of the line joining two oxygen atoms in a 1,4-dioxane to the *ab* plane is nearly parallel to one of the diagonals of the *ab* plane, and the dihedral angles between the mean plane of 1,4-dioxane and the *ab* plane is about 49.4°. All of 1,4-dioxane molecules surround the linear Co(II) hydrogen-bonding chain *via* hydrogen bonds to form a 3-D hydrogen-bonding network (Fig. 3c).

4 crystallizes in monoclinic with space group *C* 2/c. One and two of half Co(II), eight H_2O, four monodentate Br^-, two and four of half 1,4-dioxane molecules coexist in an independent unit. Each Co(II) center adopts a regular octahedral geometry. The coordination sphere is completed by two monodentate Br^- with Co–Br 2.620(1)–2.624(1) Å and two H_2O in the basal plane, and two H_2O at the axial sites with Co–O 2.058(5)–2.080(5) Å (Fig. 4a). In **4**, the neighboring mononuclear $CoBr_2(H_2O)_4$ compounds interact with each other *via* hydrogen bonds between Br^- and H_2O to generate a 3D diamondoid hydrogen-bonding network with a Co···Co separation of *ca.*6.70 Å (Fig. 4b and c).[17] The guest 1,4-dioxane molecules fill into the vacancies of the 3-D diamondoid network with a chair conformation *via* hydrogen bonds between H_2O and 1,4-dioxane as listed in Table 2.

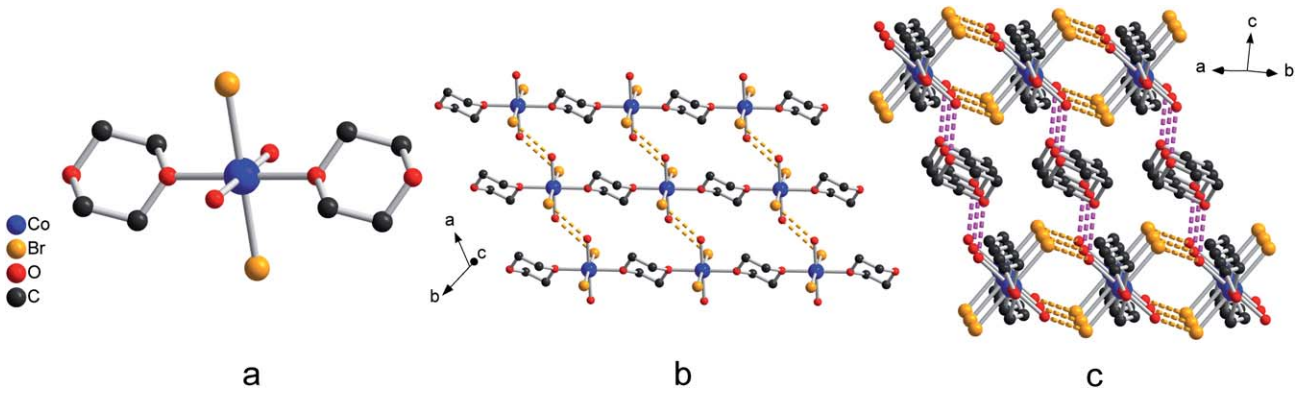

Fig. 2 a) The coordination geometry of Co(II) cation in **2**; b) 1-D Co(II)–Diox chains and a 2-D hydrogen-bonding layer in **2**; hydrogen bonds are indicated by yellow dotted lines; c) a 3-D hydrogen-bonding network in **2**; hydrogen bonds are indicated by yellow and purple dotted lines.

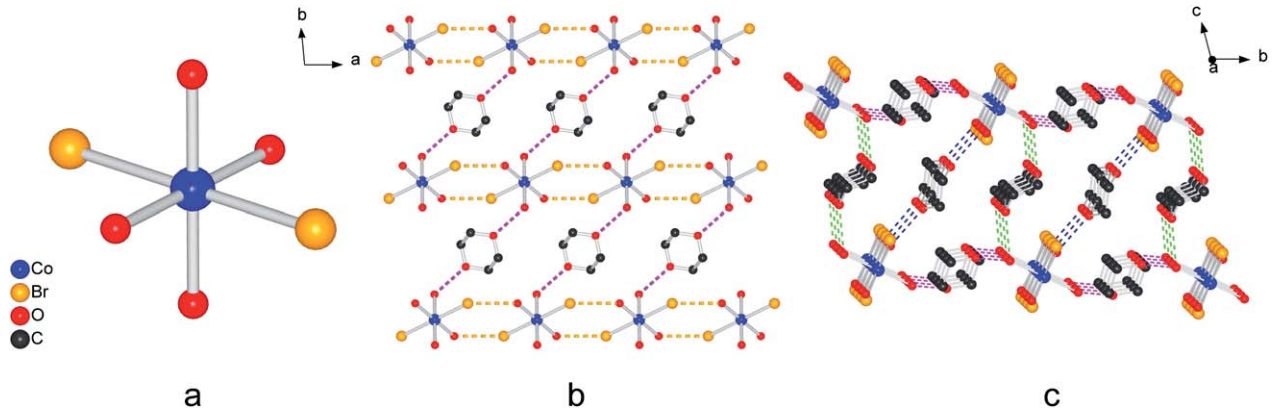

Fig. 3 a) The coordination geometry of a Co(II) cation in **3**; b) linear hydrogen-bonding chains in **3**; c) a 3-D hydrogen-bonding network in **3**; hydrogen bonds are indicated by yellow, green and purple dotted lines. Hydrogen atoms were omitted for clarity.

5 crystallizes in tetragonal with space group $I\ 4_1/a$.[11] The asymmetric unit contains a quarter of Co(II), half of monodentate Br^-, one H_2O, and half of a guest 1,4-dioxane molecule. The coordination geometry of **5** is very similar to that of **4** with Co–Br 2.6184(6) Å and Co–O 2.076(5) Å (Fig. 4a). A 3-D hydrogen-bonding network was formed through hydrogen bonds among $CoBr_2(H_2O)_4$ and guest molecule (Fig. 4b and d). The chair-conformed 1,4-dioxane molecules are orientated in two perpendicular directions and form columns along the *a* and *b* axes, separately. 1,4-dioxane column interacts with the neighboring Co(II) octahedra *via* short contacts between H_2O and1,4-dioxane molecule.

From **1** to **5**, the dimensionalities change from 2D (**1**) to 1D (**2**) and 0D (**3**, **4**, **5**). In **1**–**5**, Br^- bonds to Cu(II) monodentately, and

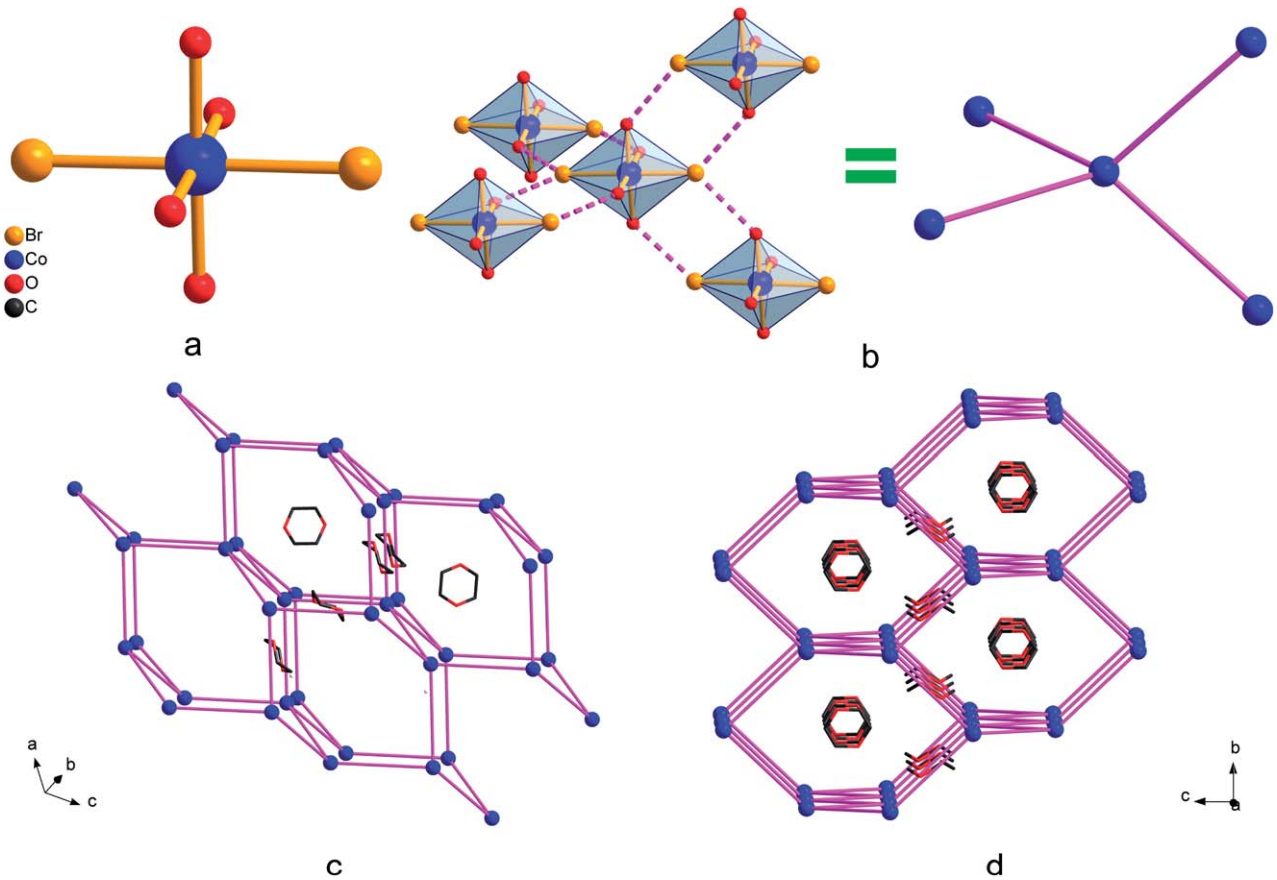

Fig. 4 a) The coordination geometry of a Co(II) cation in **4** and **5**; b) a topological unit in the 3-D diamondoid hydrogen-bonding network in **4** and **5**; c) the 3-D diamondoid hydrogen-bonding network and the arrangement of 1,4-dioxane molecules in **4**; d) the 3-D diamondoid hydrogen-bonding network and the packing modes of 1,4-dioxane molecules in **5**. Hydrogen atoms were omitted for clarity.

Co–Br distances increase from 2.540 and 2.562 Å in **1** to 2.578 Å in **2**, and ~2.620 Å in **3–5**. 1,4-dioxane molecules display different chair-conformations in **1–5**. 1,4-dioxane molecules serve as bridge ligands in **1**, terminal ligands in **2** to guest molecules in **3–5**, and the distance from Co(II) to Diox remains almost the same in **1** and **2**. From **2** to **5**, H_2O bond to Co(II) monodentately and the Co–O distances remain the same.

Our preliminary studies on the MCl_2/1,4-dioxane/H_2O system indicated that water and 1,4-dioxane molecules can tune the structure, color, and physical properties during the de/resolvation process, and the changes in hydrogen bonding upon de/resolvation can be expected.[10] Actually, the mechanism of the hydrogen bond formation or disruption may largely affect the molecular confinement, as well as the structural conformation, although they still remain ill-understood. Our attempt at working with the MBr_2/1,4-dioxane/H_2O system has demonstrated the importance of parameter selection. It is possible to obtain a family of complexes from the ternary $CoBr_2$–(1,4-dioxane)–H_2O system as shown in the isothermal phase-diagram at room temperature (Fig. 5).

In initial exploration of the crystallization behavior of $CoBr_2$ in a mixture of methanol and 1,4-dioxane we could obtain the 2D phase of **1** by slow solvent evaporation in a desiccator. Crystallization in nonaqueous media may cause the generation of

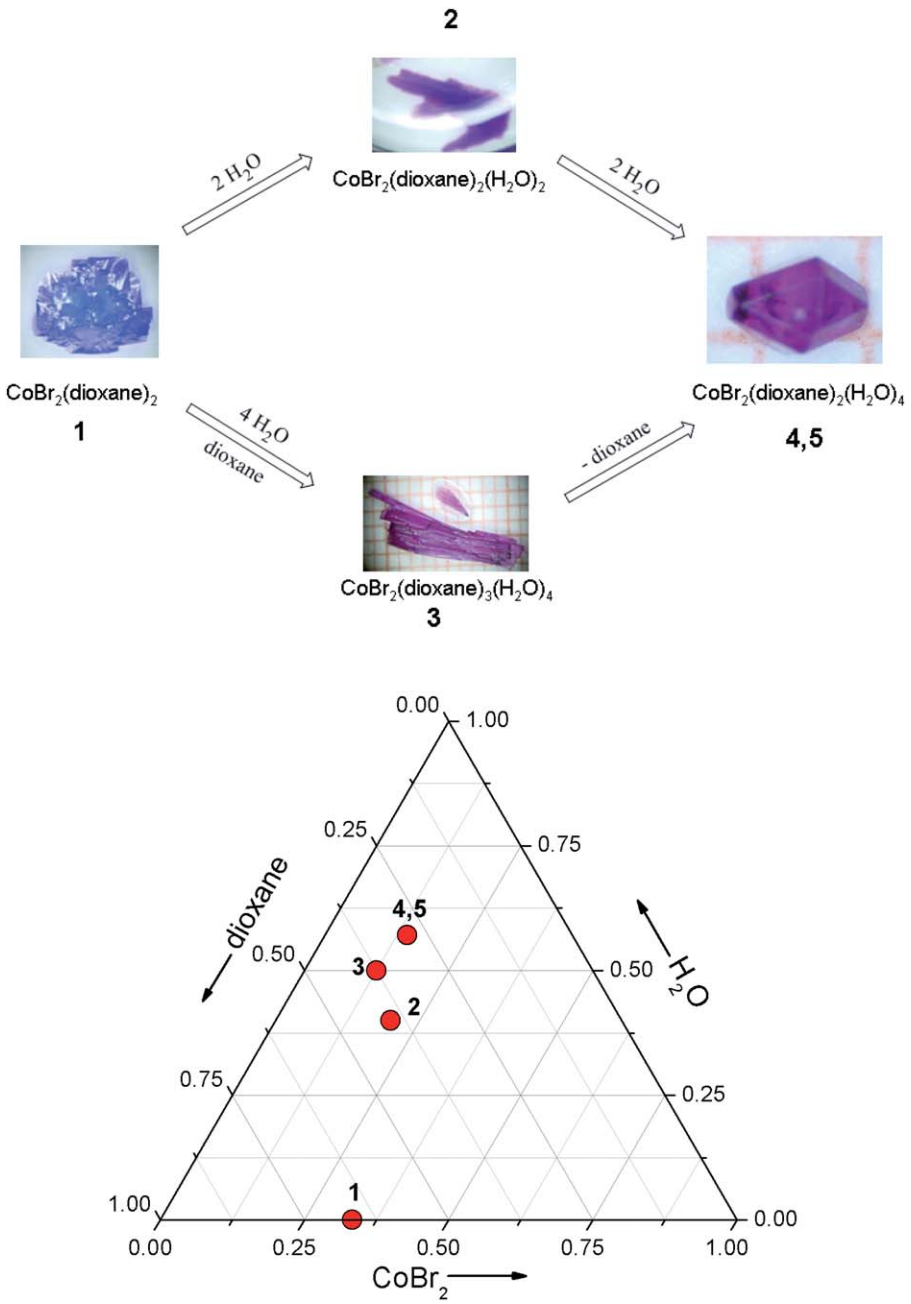

Fig. 5 a) The appearances of crystals of **1–5**, and possible routes for the solvent-mediated transformations; b) a phase diagram of the ternary $CoBr_2$–(1,4-dioxane)–H_2O system and existence of **1–5**.

1,4-dioxane coordinated species, therefore it is reasonable to expect a network without the influence of hydrogen bonds. The preferred packing mode is layer by layer in an AB fashion due to the steric hindrance of Br^- anions. When varying crystallization conditions by exposure to moisture, we observed the formation of the 1D phase of **2** and the 0D phase of **3**. The compositions of **2** and **3** are very similar only differing in the amount of 1,4-dioxane and water molecules. The 1D structure of **2** can be considered as an interruption of the 2D structure of **1** by water induced hydrogen bonds as shown in Scheme 1. The bonds between the 1,4-dioxane and Co(II) were broken by introducing water molecules in moist air, and the hydrogen bonds between Br^- anions and coordinated water molecules began to play an important role in network constructions. Through this kind of hydrogen bond, the 1D chains of **2** were connected to create robust 2D hydrogen bonding layers, while the 0D octahedrons of **3** were just linked to form 1D hydrogen bonding chains. In both cases, the loose hydrogen bonds (O–H···O) between 1,4-dioxane and coordinated H_2O molecules accounted for the formation of 3D hydrogen bonding networks. Upon standing for a relatively long time in the presence of the mother liquor and a further introduction of H_2O molecules, **2** or **3** disappeared leaving the 0D phase of **4** or **5** as in Scheme 1. Both **4** and **5** have the same composition differing only in the packing mode. A more robust 3D diamondoid hydrogen bonding network was formed by considering the hydrogen bonds between Br^- and H_2O, and there existed a tendency to establish a stable hydrogen bond network after complete substitution of the Co(II) coordination sphere by H_2O instead of 1,4-dioxane molecules. The stability of the 3D diamondoid hydrogen bonding network was also affected by the packing of guest 1,4-dioxane molecules in void spaces, therefore, the subsequent transformation between **4** and **5** occurred by the rearrangement of the 1,4-dioxane molecules.

Under selected conditions, **4** and **5** were thermodynamically stable products whose nucleations were preceded by the formation of the metastable complexes of **2** and **3**, while the crystallization of the kinetically favored species of **1** was provoked at the initial nucleation stage. Based on Ostwald's rule, different crystalline species **2–5** nucleated sequentially starting from the least stable **1**, and only the more stable **4** and **5** survived by solvent-mediated transformation process.[18] The red block crystal $CoBr_2 \cdot 6H_2O$, as the most stable phase in ternary $CoBr_2$–(1,4-dioxane)–H_2O system, was obtained when the solution was exposure to high humidity for months as in Scheme S2†.

1 is a 2D antiferromagnet with a critical temperature (T_N) of 3.0 K. The temperature dependence of the magnetic susceptibility of **1** in an applied field of 1000 Oe displays mainly antiferromagnetic character. At room temperature, the χT value of 3.26 cm^3 K mol^{-1} is close to that expected for the Co^{2+} ion, significantly larger than the expected value (1.875 cm^3 K mol^{-1}) for the isolated, spin-only ion with $S = 3/2$ and $g = 2.00$. This is expected for the Co^{2+} ion owing to the significant orbital contribution of Co^{2+} ion with strong spin–orbit coupling in an octahedral environment as 2.80 cm^3 K mol^{-1} in $Co(C_2O_4)(HO(CH_2)_3OH)$, 2.82 cm^3 K mol^{-1} in $A_2[Co_2(C_2O_4)_3]$ (A = ammonium salt derived from diethylenetriamine) and others.[19] The χT values decrease slowly upon cooling, and reach a minimum of 1.91 cm^3 K mol^{-1} at around 6–7 K (Fig. 6). After the minimum, the χT values show a little change in the range of 3–6 K, and then

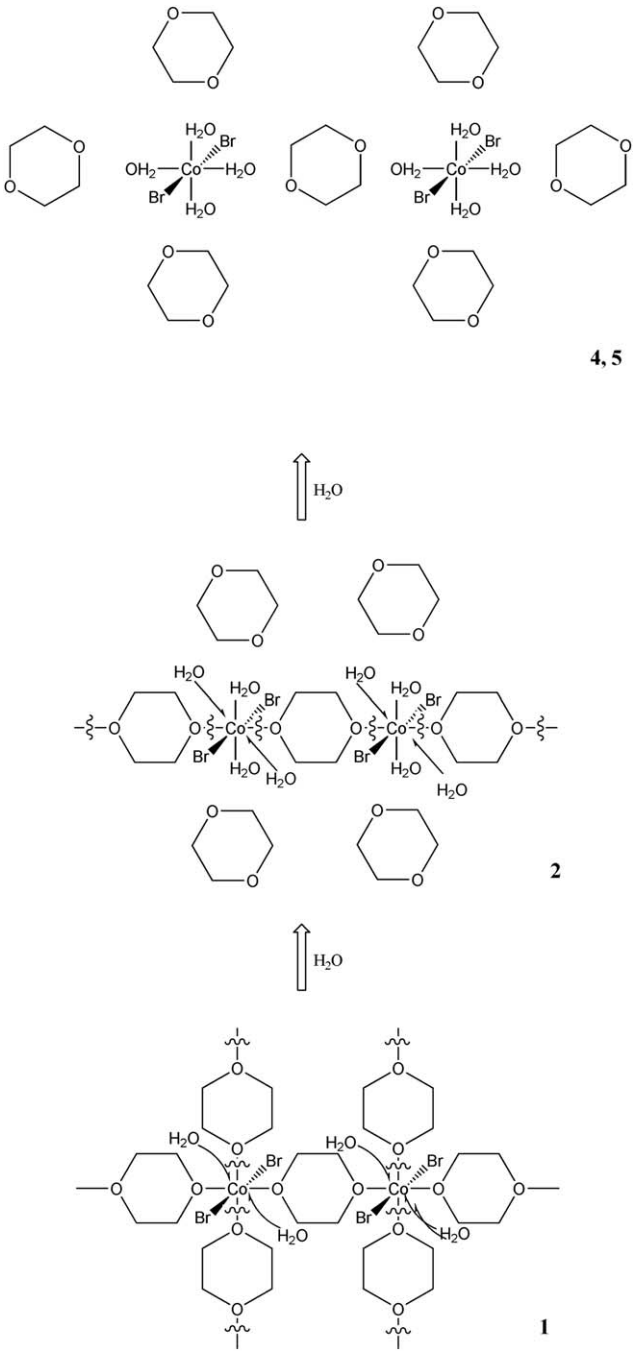

Scheme 1 A schematic drawing of the possible route of crystal-to-crystal transformation from **1** to **2** and **4**, **5**.

display a rise to 1.99 cm^3 K mol^{-1} at 2.0 K. The χ^{-1} *vs.* T data above 50 K can be well fitted to the Curie–Weiss law with $C =$ 3.61 cm^3 K mol^{-1} and $\theta = -30.7$ K. The negative Weiss temperature indicated the antiferromagnetic interaction between the Co^{2+} ions. Zero-field-cooled and field-cooled magnetization (ZFCM/FCM) under 10 Oe shows a bifurcation at 2.9 K, and FCMs reached ~16 cm^3 G mol^{-1} at 2 K. Remanent magnetization (RM) indicated the spontaneous magnetization as a weak ferromagnetism or canted antiferromagnetism.[20] The T_N value of 2.9 K in **1** is lower than those values observed in other 2-D (4,4)

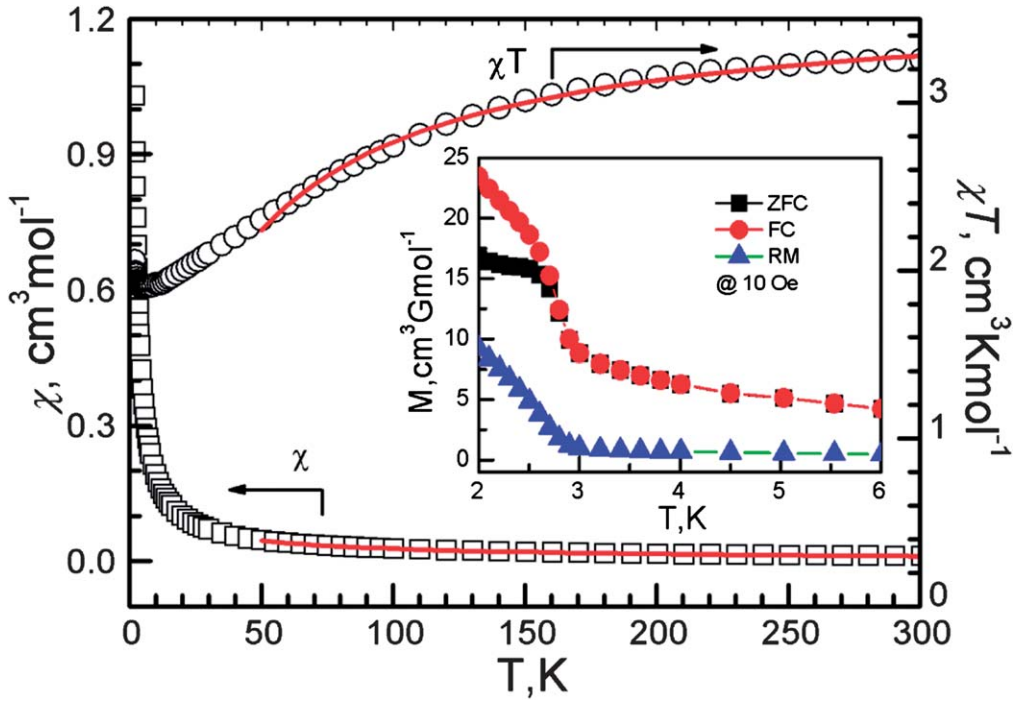

Fig. 6 χ *vs.* T and χT *vs.* T plots of **1** under 1000 Oe; red solid lines are fits to the Curie–Weiss law. Insert: ZFC/FC/RM at 10 Oe.

topological networks.[21]The isothermal magnetizations at 2 K display an increase with the increased field and reach a plateau at *ca.* 30 kOe. The magnetization reaches *ca.* 2.44 $N\beta$ at 60 kOe, which is lower than the saturation value of 3 $N\beta$ for Co^{2+} ($S = 3/2$ and $g = 2.00$). In a very low field region, the magnetizations showed no hysteresis loop, and this behavior needs further investigations.

The temperature dependence of magnetic susceptibility measured in an applied field of 1000 Oe for **3** shows mainly antiferromagnetic character. The χ value only shows a maximum of 0.20 $cm^3\ mol^{-1}$ at *ca.* 3.4 K, and the χT values decrease slowly upon cooling (Fig. 7). At 300 K, the χT value of 3.29 $cm^3\ K\ mol^{-1}$ is expected for the Co^{2+} ion.[18] The susceptibility data above 50 K can be well fitted by the Curie–Weiss law with $C = 3.52\ cm^3\ K\ mol^{-1}$ and $\theta = -24.4$ K. The χT values show a discontinuity of 0.66 $cm^3\ K\ mol^{-1}$ around 3.4 K followed by another decrease to 0.34 $cm^3\ K\ mol^{-1}$ at 2.0 K. In fact, the FC magnetizations under 10 Oe field display a maximum peak at 3.4 K, and a further

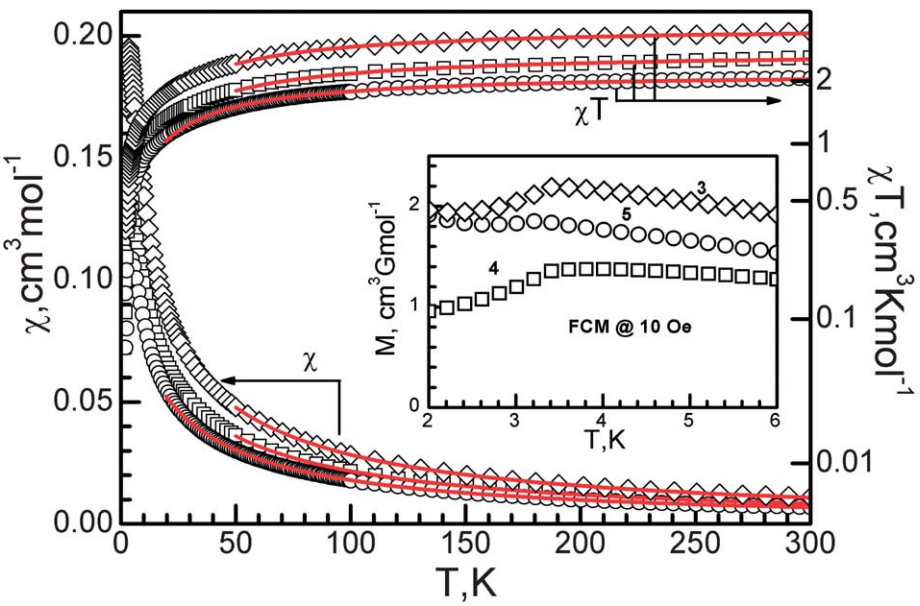

Fig. 7 χ *vs.* T and χT *vs.* T plots of **3**, **4** and **5** under 1000 Oe; red solid lines are fits to the Curie–Weiss law. Insert: FC of **3**, **4** and **5** at 10 Oe.

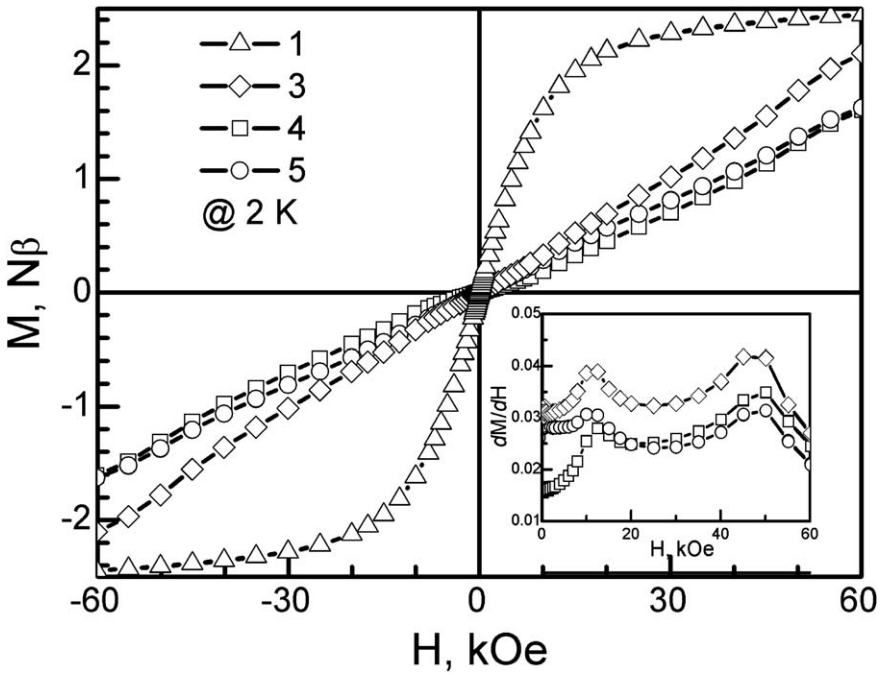

Fig. 8 Isothermal magnetization plots of **1**, and **3–5** at 2 K. Insert: d*M*/d*H* plots of **3–5**.

decrease below 3.4 K. In the isothermal magnetizations at 2.0 K, no hysteresis is observed, and the magnetization reaches *ca.* 2.10 $N\beta$ at 60 kOe.

The magnetic behavior of **4** suggests the AF ordering. The χ value only shows a maximum of 0.13 $cm^3\ mol^{-1}$ at *ca.* 4.0 K, and the χT values decrease slowly upon cooling. At 300 K, the χT value is 2.54 $cm^3\ K\ mol^{-1}$. The susceptibility data above 50 K can be fitted by the Curie–Weiss law well with $C = 2.74\ cm^3\ K\ mol^{-1}$ and $\theta = -26.8$ K. The FC magnetizations under 10 Oe field display a maximum peak at 3.8 K, and a further decrease below 3.8 K. In the isothermal magnetization measurement at 2 K, **4** shows no noticeable hysteresis, and the magnetization reaches at *ca.* 1.61 $N\beta$ at 60 kOe (Fig. 8) being significantly lower than the saturation value of 3 $N\beta$ for Co^{2+} ($S = 3/2$ and $g = 2.00$) and higher than 1 $N\beta$ for low-spin Co^{2+} with $S = 1/2$ and $g = 2.00$. Interestingly, two well defined peaks at *ca.* 12.5 kOe and 50 kOe are observed in the d*M*/d*H*-*H* plot at 2.0 K, corresponding to the fields of spin-flop transition (AF-SP) and the transition from flopped to the paramagnetic phase.[22] This magnetic behavior is reminiscent of a perovskite Fe-formate $[C(NH_2)_3][Fe(HCOO)_3]$.[2k]

The magnetic behavior of **5** is similar to that of **4**. The χ value only shows a maximum of 0.11 $cm^3\ mol^{-1}$ at *ca.* 3.5 K, and the χT values decrease slowly upon cooling. At 300 K, the χT value of 2.06 $cm^3\ K\ mol^{-1}$ is expected for the value 1.875 $cm^3\ K\ mol^{-1}$ as isolated, spin-only Co^{2+} ion with $S = 3/2$ and $g = 2.00$. The susceptibility data above 50 K can be fitted by the Curie–Weiss law well with $C = 2.22\ cm^3\ K\ mol^{-1}$ and $\theta = -23.9$ K. The FC magnetizations under 10 Oe field display a maximum peak at 3.4 K, and a further decrease below 3.4 K. In the isothermal magnetization measurement at 2 K, no noticeable hysteresis is observed, and the magnetization reaches at *ca.* 1.63 $N\beta$ at 60 kOe being significantly lower than the saturation value of 3 $N\beta$ for Co^{2+} ($S = 3/2$ and $g = 2.00$). The field (H_{SF}) for AF-SP transition and the critical field ($H_{SP\text{-}P}$) for the SP-P transition are also reflected in two well defined peaks at *ca.* 10.0 kOe and 50 kOe in the d*M*/d*H*-*H* plot at 2.0 K.

From **3** to **5**, the χT values at room-temperature decreased from 3.29, 2.54 to 2.06 $cm^3\ K\ mol^{-1}$ while Curie constants decreased from 3.52, 2.74 to 2.22 $cm^3\ K\ mol^{-1}$ and the Weiss constants remained the same, it shows that spin–orbit coupling in Co^{2+} ion decreased from **3** to **5**, and the hydrogen bonds between coordination molecules play an important role in magnetic properties.

Conclusions

We have investigated that kinetically favored **1** can be converted into metastable species **2** and **3**, and finally transformed into thermodynamically stable species **4** and **5**. Some kinetic and thermodynamical factors influencing the self-assembly of the network and phase transformation during the crystallization process have been discussed. The hydrogen bond formation or disruption plays an important role in the network crystallization and molecular magnetization. Based on the present work, a further investigation of the nature of the crystallization process is necessary, and it is possible to obtain new types of hydrogen bonding networks by fine tuning the synthetic and crystallization conditions.

Acknowledgements

The authors thank Prof. Zheming Wang, Song Gao of College of Chemistry and Molecular Engineering, Peking University, for their kind help in X-ray experiments and valuable discussions. This work was supported by NSFC No. 20873154, 21173230 and MOST 2011CB932302 of China.

References

1 O. K. Farha and J. T. Hupp, *Acc. Chem. Res.*, 2010, **43**, 1166; S. Horike, S. Shimomura and S. Kitagawa, *Nat. Chem.*, 2009, **1**, 695; *Chem. Soc. Rev.*, 2009, **38**, 1201; M. O'Keeffe, M. A. Peskov, S. J. Ramsden and O. M. Yaghi, *Acc. Chem. Res.*, 2008, **41**, 1782; D. Bradshaw, J. E. Warren and M. J. Rosseinsky, *Science*, 2007, **315**, 977; G. Ferey, C. Mellot-Draznieks, C. Serre and F. Millange, *Acc. Chem. Res.*, 2005, **38**, 217; N. W. Ockwig, O. Delgado-Friedrichs, M. O'Keeffe and O. M. Yaghi, *Acc. Chem. Res.*, 2005, **38**, 176; S. Kitagawa, R. Kitaura and S. Noro, *Angew. Chem., Int. Ed.*, 2004, **43**, 2334.

2 H. Furukawa, N. Ko, Y. B. Go, N. Aratani, S. B. Choi, E. Choi, A. O. Yazaydin, R. Q. Snurr, M. O'Keeffe, J. Kim and O. M. Yaghi, *Science*, 2010, **239**, 424; D. Yuan, D. Zhao, D. Sun and H.-C. Zhou, *Angew. Chem., Int. Ed.*, 2010, **49**, 5357; L. J. Murray, M. Dincă, J. Yano, S. Chavan, S. Bordiga, C. M. Brown and J. R. Long, *J. Am. Chem. Soc.*, 2010, **132**, 7856; F. Song, C. Wang, J. M. Falkowski, L. Ma and W. Lin, *J. Am. Chem. Soc.*, 2010, **132**, 15390; L. Q. Ma, C. Abney and W. B. Lin, *Chem. Soc. Rev.*, 2009, **38**, 1248; J. Lee, O. K. Farha, J. Roberts, K. A. Scheidt, S. T. Nguyen and J. T. Hupp, *Chem. Soc. Rev.*, 2009, **38**, 1450; C. Valente, E. Choi, M. E. Belowich, C. J. Doonan, Q. Li, T. B. Gasa, Y. Y. Botros, O. M. Yaghi and F. Stoddart, *Chem. Commun.*, 2010, **46**, 4911; Z. Xie, L. Ma, K. E. deKrafft, A. Jin and W. Lin, *J. Am. Chem. Soc.*, 2010, **132**, 922; O. R. Evans and W. Lin, *Acc. Chem. Res.*, 2002, **35**, 511; M. Kurmoo, *Chem. Soc. Rev.*, 2009, **38**, 1353; Z. Wang, K. Hu, S. Gao and H. Kobayashi, *Adv. Mater.*, 2010, **22**, 1526; P. Jain, V. Ramachandran, R. J. Clark, H. D. Zhou, B. H. Toby, N. S. Dalal, H. W. Kroto and A. K. Cheetham, *J. Am. Chem. Soc.*, 2009, **131**, 13625.

3 D. Braga and F. Grepioni, *Acc. Chem. Res.*, 2000, **33**, 601; *Crystal Engineering: The Design and Application of Functional Solids, NATO, ASI series*, ed. K. R. Seddon and M. Zaworotko, Kluwer Academic Publishers, Dordrecht, 1999; *Crystal Engineering: The Design of Organic Solids*, ed. G. R. Desiraju, Elsevier, Amsterdam, 1989.

4 T. Steiner, *Angew. Chem., Int. Ed.*, 2002, **41**, 48; *Crystal Design: Structure and Function; Perspectives in Supramolecular Chemistry*, ed. G. R. Desiraju, John Wiley & Sons, Chichester, 2003; M. Alajarin, A. E. Aliev, A. D. Burrows, K. D. M. Harris, A. Pastor, J. W. Steed and D. R. Turner, in *Supramolecular Assembly* Via *Hydrogen Bonds I & II; Structure and Bonding*, ed. D. M. P. Mingos, Springer-Verlag, Berlin, 2004, Vols 108 & 111.

5 K. L. Hu, M. Kurmoo, Z. M. Wang and S. Gao, *Chem.–Eur. J.*, 2009, **15**, 12050; D. K. Kumar, A. Das and P. Dastidar, *Cryst. Growth Des.*, 2006, **6**, 1903; J. Lu, J. H. Yu, X. Y. Chen, P. Cheng, X. Zhang and J. Q. Xu, *Inorg. Chem.*, 2005, **44**, 5978; Y. Wang, J. Yu, Y. Li, Z. Shi and R. Xu, *Chem.–Eur. J.*, 2003, **9**, 5048.

6 C. A. Wheaton, M. C. Jennings and R. J. Puddephatt, *J. Am. Chem. Soc.*, 2006, **128**, 15370; C. Livage, C. Egger and G. Ferey, *Chem. Mater.*, 2001, **13**, 410; M. D. Levin and P. J. Stang, *J. Am. Chem. Soc.*, 2000, **122**, 7428.

7 G. M. Espallargas, J. van de Streek, P. Fernandes, A. J. Florence, M. Brunelli, K. Shankland and L. Brammer, *Angew. Chem., Int. Ed.*, 2010, **49**, 8892; S. M. Hawxwell, G. M. Espallargas, D. Bradshaw, M. J. Rosseinsky, T. J. Prior, A. J. Florence, J. van de Streek and L. Brammer, *Chem. Commun.*, 2007, 1532.

8 J. J. Zhang, C. S. Day and A. Lachgar, *CrystEngComm*, 2011, **13**, 133; S. V. Potts and L. J. Barbour, *New J. Chem.*, 2010, **34**, 2451; L. T. Higham, U. P. Kreher, R. J. Mulder, C. R. Straussa and J. L. Scott, *Chem. Commun.*, 2004, 2264.

9 L. Carlucci, G. Ciani, J. M. García-Ruiz, M. Moret, D. M. Proserpio and S. Rizzato, *Cryst. Growth Des.*, 2009, **9**, 5024; L. Carlucci, G. Ciani, M. Moret, D. M. Proserpio and S. Rizzato, *Chem. Mater.*, 2002, **14**, 12.

10 B. Zhang, D. Zhu and Y. Zhang, *Chem.–Asian J.*, 2011, **6**, 1367; B. Zhang, D. B. Zhu and Y. Zhang, *Chem.–Eur. J.*, 2010, **16**, 9994; Z. Duan, B. Zhang, Y. Zhang and D. B. Zhu, *J. Am. Chem. Soc.*, 2009, **131**, 6934.

11 J. C. Barnes and T. J. R. Weakley, *J. Chem. Soc. Dalton Trans.*, 1986, 1786.

12 Otwinowski and Minor, *Denzo and Scalepack*, 1997; Rigaku Inc, *CrystalClear*, 2007.

13 G. M. Sheldrick, *SHELXS-97*, University of Göttingen: Germany, 1997.

14 O. Kahn, *Molecular Magnetism*, Wiley, New York, 1993; R. L. Carlin and A. L. van Duyneveldt, *Magnetic Properties of Transition Metal Compounds*, Springer, New York, 1997.

15 H. L. Gao, L. Yi, B. Zhao, X. Q. Zhao, P. Cheng, D. Z. Liao and S. P. Yan, *Inorg. Chem.*, 2006, **45**, 5980; J. Pasán, J. Sanchiz, C. Ruiz-Pérez, F. Lloret and M. Julve, *Inorg. Chem.*, 2005, **44**, 7794; M. L. Tong, B. H. Ye, W. J. Cai, M. X. Chen and S. W. Ng, *Inorg. Chem.*, 1998, **37**, 2645.

16 T. Hong, R. Custelcean, B. C. Sales, B. Roessli, D. K. Singh and A. Zheludev, *Phys. Rev. B: Condens. Matter Mater. Phys.*, 2009, **80**, 132404.

17 O. Saied, T. Maris, X. Wang, M. Simard and J. D. Wuest, *J. Am. Chem. Soc.*, 2005, **127**, 10008; B. Q. Ma, H. L. Sun and S. Gao, *Inorg. Chem.*, 2005, **44**, 837; S. V. Lindeman, J. Hecht and J. K. Kochi, *J. Am. Chem. Soc.*, 2003, **125**, 11597; V. A. Russell and M. D. Ward, *Chem. Mater.*, 1996, **8**, 1654; M. J. Zaworotko, *Chem. Soc. Rev.*, 1994, **23**, 283.

18 W. Ostwald, *Z. Phys. Chem.*, 1897, **22**, 289; A. Michaelides and S. Skoulika, *Cryst. Growth Des.*, 2009, **9**, 2039; D. Croker and B. K. Hodnett, *Cryst. Growth Des.*, 2010, **10**, 2806.

19 Z. Duan, Y. Zhang, B. Zhang and D. Zhu, *Inorg. Chem.*, 2008, **47**, 9152; Z. Duan, Y. Zhang, B. Zhang and F. Pratt, *Inorg. Chem.*, 2009, **48**, 2140; R. L. Carlin and A. L. van Duyneveldt, *Magnetic Properties of Transition Metal Compounds*, Springer-Verlag, New York, 1977; pp 69–71.

20 B. Zhang, Y. Zhang, J. Zhang, J. Li and D. Zhu, *Dalton Trans.*, 2008, 5037; Z. M. Wang, B. Zhang, K. Inoue, H. Fujiwara, T. Otsuka, H. Kobayashi and M. Kurmoo, *Inorg. Chem.*, 2007, **46**, 437; Z. M. Wang, B. Zhang, H. Fujiwara, H. Kobayashi and M. Kurmoo, *Chem. Commun.*, 2004, 416; Z. M. Wang, B. Zhang, T. Otsuka, K. Inoue, H. Kobayashi and M. Kurmoo, *Dalton Trans.*, 2004, 2209.

21 O. Fabelo, J. Pasán, L. Cañadillas-Delgado, F. S. Delgado, F. Lloret, M. Julve and C. Ruiz-Pérez, *Inorg. Chem.*, 2009, **48**, 6086.

22 J. L. Manson, C. R. Kmety, F. Palacio, A. J. Epstein and J. S. Miller, *Chem. Mater.*, 2001, **13**, 1068; B. Q. Ma, H. L. Sun, S. Gao and G. Su, *Chem. Mater.*, 2001, **13**, 1946; M. Yuan, S. Gao, H. L. Sun and G. Su, *Inorg. Chem.*, 2004, **43**, 8221; X. Y. Wang, L. Wang, Z. M. Wang, G. Su and S. Gao, *Chem. Mater.*, 2005, **17**, 6369; M. Yuan, F. Zhao, W. Zhang, Z. M. Wang and S. Gao, *Inorg. Chem.*, 2007, **46**, 11235.

